Journal of Human Evolution 159 (2021) 103049

Contents lists available at ScienceDirect

Journal of Human Evolution

journal homepage: www.elsevier.com/locate/jhevol

Effects of hybridization on pelvic morphology: A macaque model

Laura T. Buck [a, b, *], David C. Katz [b, c], Rebecca Rogers Ackermann [d, e], Leslea J. Hlusko [f, g], Sree Kanthaswamy [h], Timothy D. Weaver [b]

[a] School of Biological and Environmental Sciences, Liverpool John Moores University, UK
[b] Department of Anthropology, University of California Davis, USA
[c] University of Calgary, Cumming School of Medicine, Canada
[d] Department of Archaeology, University of Cape Town, South Africa
[e] Human Evolution Research Institute, University of Cape Town, South Africa
[f] Department of Integrative Biology, University of California Berkeley, USA
[g] Centro Nacional de Investigación sobre la Evolución Humana (CENIEH), Burgos, Spain
[h] School of Natural and Mathematical Sciences, Arizona State University, USA

ARTICLE INFO

Article history:
Received 10 November 2020
Accepted 25 June 2021
Available online xxx

Keywords:
Hybridization
Human evolution
Primate
Skeletal morphology
Geometric morphometric methods
Macaca mulatta

ABSTRACT

Ancient DNA analyses have shown that interbreeding between hominin taxa occurred multiple times. Although admixture is often reflected in skeletal phenotype, the relationship between the two remains poorly understood, hampering interpretation of the hominin fossil record. Direct study of this relationship is often impossible due to the paucity of hominin fossils and difficulties retrieving ancient genetic material. Here, we use a sample of known ancestry hybrids between two closely related nonhuman primate taxa (Indian and Chinese *Macaca mulatta*) to investigate the effect of admixture on skeletal morphology. We focus on pelvic shape, which has potential fitness implications in hybrids, as mismatches between maternal pelvic and fetal cranial morphology are often fatal to mother and offspring. As the pelvis is also one of the skeletal regions that differs most between *Homo sapiens* and Neanderthals, investigating the pelvic consequences of interbreeding could be informative regarding the viability of their hybrids. We find that the effect of admixture in *M. mulatta* is small and proportional to the relatively small morphological difference between the parent taxa. Sexual dimorphism appears to be the main determinant of pelvic shape in *M. mulatta*. The lack of difference in pelvic shape between Chinese and Indian *M. mulatta* is in contrast to that between Neanderthals and *H. sapiens*, despite a similar split time (in generations) between the hybridizing pairs. Greater phenotypic divergence between hominins may relate to adaptations to disparate environments but may also highlight how the unique degree of cultural buffering in hominins allowed for greater neutral divergence. In contrast to some previous work identifying extreme morphologies in first- and second-generation hybrids, here the relationship between pelvic shape and admixture is linear. This linearity may be because most sampled animals have a multigenerational admixture history or because of relatively high constraints on the pelvis compared with other skeletal regions.

1. Introduction

Elucidating the effects of hybridization is critical for understanding the context of human evolution and the processes driving it (Ackermann et al., 2016). The past few years have seen great methodological advances in ancient DNA (aDNA) analyses, enabling the detection of interbreeding events and resulting in an increased appreciation of their frequency and importance (for reviews, refer to Gopalan et al., 2021; Wolf and Akey, 2018). Despite these advances, we are still far from understanding the importance of gene flow between hominin lineages in determining morphology and from recognizing hybrids in the fossil record (Warren et al., 2018). Claims of hybrid Neanderthal/*Homo sapiens* fossils were made for decades before supporting genetic evidence was available (Duarte et al., 1999; Trinkaus et al., 2003a, 2003b; Rougier et al., 2007). When the data are limited to fossil material and its archaeological context, however, these assertions are almost inevitably subject to

* Corresponding author.
E-mail address: l.buck@ljmu.ac.uk (L.T. Buck).

https://doi.org/10.1016/j.jhevol.2021.103049

counterclaims, such as those asserting that intermediate morphology is within the boundaries of intraspecific variation in *H. sapiens* (e.g., Tattersall and Schwartz, 1999).

In many cases, even now, preservation issues mean there is limited potential for aDNA evidence to resolve the question of which putative (morphological) hybrids are actual (genetic) hybrids. There have nonetheless been some spectacular finds. One such was the aDNA analysis of the Oase 1 mandible from Romania, which showed that this *H. sapiens* individual did indeed have a recent Neanderthal ancestor (Fu et al., 2015), as had been suggested from its morphology (Trinkaus et al., 2003a, 2003b; Rougier et al., 2007). Although the exact relationship between Oase 1's hybrid ancestry and suggested Neanderthal traits is not clear, the fact that it was identified as a hybrid based on both morphology and genetics supports a growing body of research, indicating that signatures of hybridization are detectable in skeletal morphology.

Here, we build on existing research using nonhuman primates to inform our understanding of hominin hybrids (e.g., Ackermann et al., 2006, 2014; Boel et al., 2019; Martinez et al., 2019). We use a large sample of captive full-bred and admixed Chinese and Indian rhesus macaques (*Macaca mulatta*) to elucidate the expected morphological consequences of admixture between closely related primate species, including hominins. Of particular interest because Chinese and Indian *M. mulatta* have been mixing in this captive colony for decades, the study also examines how admixture effects on phenotype vary with ancestry contributions from the two subspecies lines.

1.1. The effects of hybridization on the pelvis

We focus on the effects of hybridization on pelvic morphology. In some primates, these effects may be particularly acute due to interactions between the functional and physiological constraints of locomotion and parturition (Trevathan, 2015; Kawada et al., 2020). The pelvis is also a region of divergent shape in *H. sapiens* and *H. neanderthalensis* (Rak and Arensburg, 1987; Weaver and Hublin, 2009). Combined with neonatal crania that, although less distinct than the adult crania of these taxa, are also differently shaped (Ponce de León and Zollikofer, 2001; Gunz et al., 2012), this could have had implications for the viability of hybrid offspring. A more Neanderthal-like fetal cranium and a more *H. sapiens*-like birth canal could have led to increased likelihood of dystocia and the potential death of both mother and child. These severe consequences would have constituted a strong selective pressure likely to shape morphology, as has been suggested for the effect of caesarean sections on fetopelvic disproportion in recent humans (Mitteroecker et al., 2016, 2017). To the best of our knowledge, the relationship between pelvic morphology and admixture in the fossil record has not yet been addressed, most likely due to the paucity of both suitable well-preserved fossils and postcranial material from extant known hybrids. Thus, it is a skeletal region from which we might learn a considerable amount, regarding the morphological impact of hybridization, by adopting an approach based on nonhuman primate analogs.

1.2. Macaca mulatta *taxonomy*

The genus *Macaca* is divided into four species groups. The *fascicularis* group, which contains *M. mulatta*, is the most widely distributed group (Fooden, 1976, 2006). In 2000, Fooden reported that *M. mulatta* inhabited Southeast and South Asia with a geographic range of ~15–36 N° and ~70–120 °E, although this range was historically wider and has likely been further reduced in the last two decades. Fossils show that *M. mulatta*, or a very similar precursor, was present in its current range by >40 ka, notwithstanding the last glacial maximum, which likely caused local extinctions and subsequent postglacial in-migrations in some presently inhabited regions (Fooden, 2000).

There is substantial disagreement over the systematics of *M. mulatta*, which appears to be polyphyletic: mitochondrial DNA (mtDNA) analyses cluster Chinese *M. mulatta* with *Macaca cyclopis* or *Macaca fuscata*, rather with than their supposed conspecifics, including Indian *M. mulatta* (Melnick et al., 1993; Hayasaka et al., 1996). mtDNA also suggests deep divergences between geographic groups of *M. mulatta* to at least a subspecific level, although there remains disagreement as to how many subspecies should be recognized (Zhang and Shi, 1993; Smith and Mcdonough, 2005). Indeed, the divergence between Indian and Chinese *M. mulatta* mtDNA is deeper than between some well-accepted species pairs of macaques such as *Macaca assamensis* and *Macaca thibetana* (Hayasaka et al., 1996; Smith and Mcdonough, 2005). Similar divisions between Chinese and Indian *M. mulatta* have also been found in studies of protein polymorphisms, microsatellite single nucleotide polymorphisms (SNPs), and major histocompatibility-complex (MHC) alleles (Smith and Mcdonough, 2005; Ferguson et al., 2007).

Here, we refer to Chinese and Indian *M. mulatta* as different subspecies solely to avoid more confusing terms, such as 'group' or 'population'. Our analyses are not intended to address the validity or otherwise of that taxonomic designation. The differences between extant Chinese and Indian *M. mulatta* subspecies, particularly the molecular and physiological differences, have been studied extensively due to the species' role as a biomedical model. Chinese-derived *M. mulatta* has greater genetic heterozygosity (Smith and Mcdonough, 2005; Ferguson et al., 2007; Kanthaswamy et al., 2009) and morphological diversity (Fooden, 2000) than Indian-derived animals. Indeed, Smith and Mcdonough (2005) found pairwise differences between Indian *M. mulatta* populations to be half as great as between comparable pairs of human populations, despite the extremely low levels of genetic variation in *H. sapiens* (Smith and Mcdonough, 2005). These low levels of variation may be due to a bottleneck experienced by Indian populations in their recent evolutionary past (Smith and Mcdonough, 2005; Hernandez et al., 2007; Kanthaswamy et al., 2009). Because Neanderthals also appear to have had small population sizes and low genetic diversity (Green et al., 2010; Bocquet-Appel and Degioanni, 2013), this is another way in which this *M. mulatta* cross-sample is an interesting analog for hybridization during human evolution.

Relative to the known genetic differences, the extent of morphological variation within *M. mulatta* and between Chinese and Indian groups is less clear. Fooden (e.g., 1976, 1982, 1995, 2000, 2006) argues that although there is substantial geographic variation in the phenotype, the pattern of variation within *M. mulatta* is insufficiently clear to warrant subspecific divisions (Fooden, 2000). Fooden's (1995, 2000) taxonomy is based on a conservative designation requiring at least one trait with discontinuous variation between subspecies. Many other researchers, however, have noted substantial morphological differences between Indian- and Chinese-derived animals in particular (see discussion in Fooden, 2000). For example, Chinese males are larger than Indian males, which may reflect adaptation to a colder climate, following Bergmann's rule (Bergmann, 1847; Clarke and O'Neil, 1999). Indeed, across the species' natural range, stature and mass tend to increase gradually with latitude, although there are regional exceptions to this trend (Fooden, 2000). Tail length decreases with longitude, particularly east of 95 °E, and is, therefore, longer in Indian than in Chinese *M. mulatta* (Fooden, 2000; Hamada et al., 2005). In captive-bred Chinese and Indian *M. mulatta* housed in Louisiana, USA (Tulane National Primate Research Center), there are differences in patterns of sexual dimorphism, with greater sexual dimorphism in

Chinese than in Indian monkeys (Clarke and O'Neil, 1999). These studies suggest that size, allometric shape, and patterns of sexual dimorphism may be variables that differ between the two *M. mulatta* taxa and which therefore may vary in admixed individuals.

Chinese and Indian *M. mulatta* have been isolated from one another since at least the Late Pleistocene (Zhang and Shi, 1993; Smith and Mcdonough, 2005), likely since ~162 ka, based on genetic analyses of ~1,500 SNPs (Hernandez et al., 2007). Given a generation time of approximately 7.5 years (Wolfe, 1986) and the split time of ~162 ka (Hernandez et al., 2007), about 21,600 generations passed between the divergence of Indian and Chinese *M. mulatta* and their interbreeding in the California National Primate Research Center (CNPRC) colony in the mid-1980s (see section 2.1). The same calculation for *H. sapiens* and Neanderthals depends upon more assumptions and disputed dates, but an approximate estimation of the same variables is possible. If we use a relatively conservative split date of 550–765 ka (Meyer et al., 2016), a generation length of 26–30 years (Moorjani et al., 2016), and a date for interbreeding of 47–65 ka (Sankararaman et al., 2012), the middle point of each range results in a rough estimate of 21,482 generations between divergence and interbreeding. The macaque and hominin taxa can thus be argued to have had similar degrees of divergence between taxon pairs at the time of introgression, making Chinese and Indian *M. mulatta* an interesting model for examining Neanderthal/*H. sapiens* hybridization.

1.3. Hybridization in nonhuman primates

Hybridization appears to be commonplace in the primate order, occurring in all major lineages (Cortés-Ortiz et al., 2019). Some well-established macaque species, such as *Macaca arctoides*, are even thought to have hybrid origins (Tosi et al., 2000). Ackermann and colleagues (e.g., Ackermann et al., 2006, 2014, 2019; Ackermann and Bishop, 2010) have used nonhuman primates as hominin analogs to study the potential effects of hybridization during human evolution. The majority of this work has been carried out on baboons, which are well studied, provide a good ecological analog for hominins (Jolly, 2001; for review, see Fischer et al., 2019), and are housed in several major captive colonies with known pedigree information. Ackermann et al. (2006, 2014) showed that first- and second-generation olive-yellow baboon hybrids exhibit extreme size (heterosis) and size variation outside the parental ranges. They also display high frequencies of unusual nonmetric cranial traits and dental and sutural anomalies. This body of work, supported by other research on nonhuman primate hybridization (for reviews, see Ackermann et al., 2019; Cortés-Ortiz et al., 2019), provides some important insights to underpin the present study. Notably, there is a skeletal signal of hybridization, and the effects of hybridization appear to be similar across primate taxa, albeit with an effect of phylogenetic proximity, such that more extreme hybrids are more likely to result from interbreeding between more divergent taxa. It also provides some expectations to test with our macaque data: hybrid primates generally show increased variation and heterosis compared with parent taxa.

2. Materials and methods

2.1. Sample

Our sample is composed of *M. mulatta* housed at the CNPRC, University of California, Davis. The CNPRC colony was initially composed entirely of Indian *M. mulatta*, but after a ban on exporting primates from India in 1978, the colony's managers introduced a small number of Chinese animals to maintain genetic variation within the population. The first interbreeding was recorded in 1983 (Kanthaswamy et al., 2009). Unlike many nonhuman hybrid studies, which focus on the first few hybrid generations (e.g., Ackermann et al., 2006, 2014; Savriama et al., 2018; Warren et al., 2018), interbreeding between Indian and Chinese *M. mulatta* has been occurring in this colony for at least four to five generations (based on a generation time of ~7.5 years; Wolfe, 1986). The colony now provides a sample with a distribution from full-bred Indian to full-bred Chinese animals, including many individuals with low percentages of Chinese ancestry. This range of admixture is a better representation of what we might expect in natural hybrid zones and in the hominin fossil record if hybridization leads to viable offspring (Kelaita and Cortés-Ortiz, 2013; Fuzessy et al., 2014). In effect, the Indian *M. mulatta* housed at the CNPRC are a population experiencing a relatively small amount of genetic input from another taxon (Chinese *M. mulatta*); this can be seen as analogous to a Pleistocene *H. sapiens* population undergoing a small number of time-limited interbreeding events with Neanderthals.

Our sample data consisted of 138 full-body medical computed tomography (CT) scans from adult (>6 years) *M. mulatta* housed at the CNPRC: 94 females and 44 males. Sex ratios in the CNPRC colony are deliberately kept unbalanced to reduce intramale fighting, resulting in unequal numbers of available males and females. To optimize the spread of admixture proportions (Chinese ancestry) in our sample, we included more females than males; however, we sought to maintain the same degree of female bias in both Indian and Chinese *M. mulatta* samples to the extent possible. We included 19 full-bred Indian *M. mulatta*, 17 full-bred Chinese *M. mulatta*, and hybrid animals with a range of admixture proportions (Table 1). Estimates of Chinese ancestry were obtained from the CNPRC and are constructed from pedigree records. In our aim to obtain the best range of admixture in our sample, we included individuals with some arthritis if the original morphology was sufficiently unobscured as to allow confident landmark placement (see following paragraphs); however, we removed six animals with pathological pelves from our initial sample after examination of their CT scans, leaving the final sample of 138 (Table 1).

All animals were CT scanned at the CNPRC by appropriately trained staff. CT scanning and all other experimental procedures for this study were approved by the Institutional Animal Care and Use Committee at the University of California, Davis (protocol #19057). In most cases, monkeys were sedated and scanned in vivo. Although in a few cases monkeys were scanned as cadavers, no monkeys were sacrificed for this study. As they become available, macerated skeletal remains from cadavers of animals involved in this study are being curated in the Department of Anthropology, University of California, Davis. CT scans from the sample are also freely available on request via the MorphoSource digital archive (Morphosource.org; project name: The rhesus macaque admixture project).

2.2. Data collection

Using the CT scans, in Avizo v. 9.1 Lite (Thermo Fisher Scientific, Waltham), we virtually segmented the skeleton from the other tissue types and the pelvis from the rest of the skeleton using a

Table 1
Breakdown of sample ($n = 138$) by Chinese ancestry and sex.

Ancestry category	0%	12.5%	25%	37.5%	50%	62.5%	75%	87.5%	100%
Female	11	29	15	12	5	3	7	1	11
Male	8	15	8	3	2	2	0	0	6
Total	19	44	23	15	7	5	7	1	17

Ancestry category reflects the percentage of Chinese ancestry: 0% Chinese ancestry = full-bred Indian, 100% Chinese ancestry = full-bred Chinese. Full-bred sample $n = 36$.

mixture of automatic and manual thresholding and segmentation tools. To collect landmark coordinates for analyses using geometric morphometric methods (GMM), we digitized landmarks and semilandmarks on virtual reconstructions (shaded isosurfaces and transparent volume renderings) using Avizo and exported the coordinates for analysis in R v. 3.5.2–3.6.3 (R Core Team, 2020). We collected 48 true landmarks plus semilandmarks describing seven curves by digitizing many points along each curve (Fig. 1; Table 2). These curve semilandmarks then were resampled in R using a custom script (Supplementary Online Material [SOM]) so that each curve contained the same number of semilandmarks for each individual as follows: curve 1 (40 semilandmarks), curves 2 and 3 (18 semilandmarks each), curves 4 and 5 (30 landmarks each), and curves 6 and 7 (10 landmarks each; Fig. 2). After processing, our data set consisted of 204 total landmarks: 48 true landmarks and 156 semilandmarks. We selected landmarks and semilandmarks with the intent to optimally characterize the size and shape of the pelvis. We examined intraobserver error by using ten repetitions each of two individuals digitized repeatedly, with more than a day elapsing between each digitizing session. We processed each landmark configuration as described in the following paragraphs and compared the Procrustes distances between iterations of the same individual versus those between different individuals (see Results).

2.3. Methods of analysis

All analyses were carried out in R v. 3.5.2–3.6.3 (R Core Team, 2020) using the geomorph (Collyer and Adams, 2018, 2020; Adams et al., 2020) and Morpho (Schlager, 2017) packages and base R functions (SOM). To register the shape data, we used the procSym function in Morpho (Schlager, 2017) to perform a generalized Procrustes superimposition of the landmarks, to slide the semilandmarks along their curves using a criterion of minimizing bending energy, and to project the superimposed configurations into a tangent space. We performed principal component analysis (PCA) in geomorph (using the plotTangentSpace function) to summarize the high-dimensional data into axes of greatest explanatory power and to visualize variation within and between groups of interest on these axes. We then used geomorph's procD.lm function to perform Procrustes analysis of variance (ANOVA) to test for relationships between predictor and response variables of interest and to compare model fits. To test for the presence of different patterns of sexual dimorphism in different admixture groups, we compared the fit of additive (shape ~ admixture + sex) and interactive (shape ~ admixture * sex) models of shape, sex, and admixture. We also included a three-knot B spline model of admixture and sex-adjusted shape in the comparison to investigate whether departures from a linear

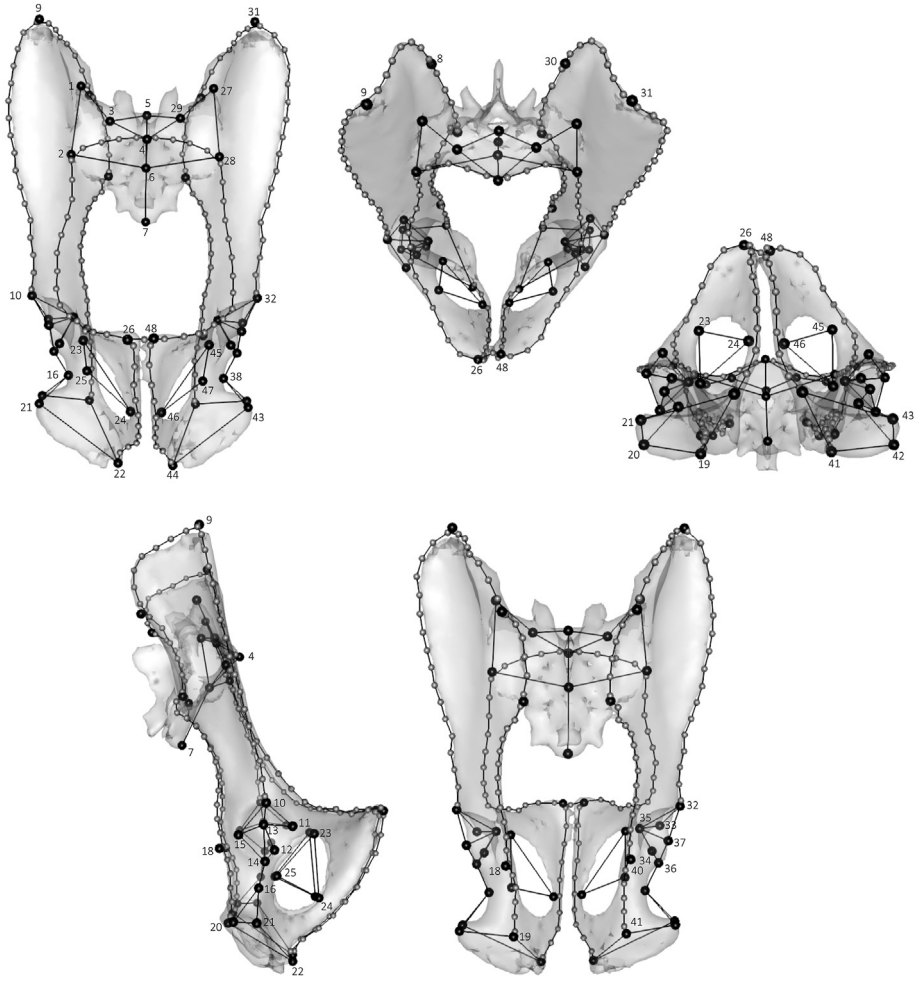

Figure 1. Landmarks and semilandmarks used in the analyses presented here viewed from (clockwise from top left) ventral, cranial, caudal, dorsal, and right lateral views. Black spheres: true landmarks, gray spheres: semilandmarks, lines: wireframe connecting landmarks and semilandmarks. For landmarks that correspond to numbers, refer to Table 2. For ease of visualization, only true landmarks are numbered, and they are numbered only in the view where they are most easily seen. In the visualization of results throughout the remaining article, only the wireframes are shown to better visualize differences between shapes.

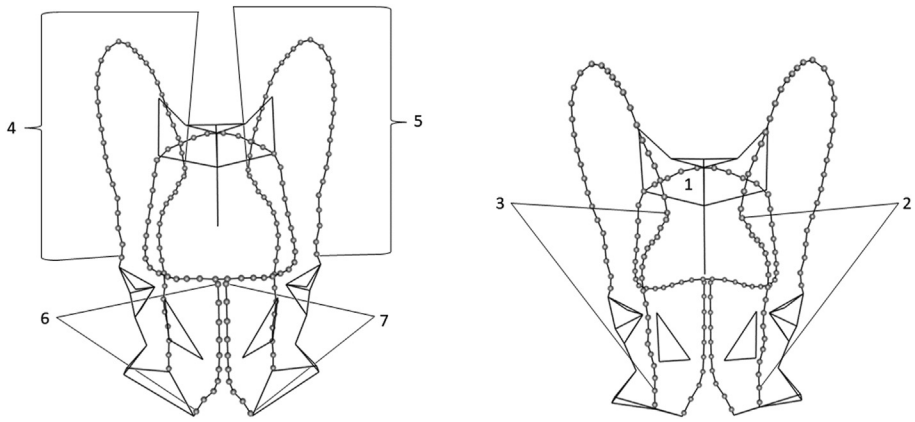

Figure 2. Semilandmark curves and wireframe used in the analyses presented here, viewed from (left to right) anterior and posterior. 1: pelvic inlet (closed) curve, 2: right dorsal ischial curve, 3: left dorsal ischial curve, 4: right iliac blade curve, 5: left iliac blade curve, 6: right pubic symphysis curve, 7: left pubic symphysis curve.

relationship between sex and ancestry could result from genetic factors such as dominance or epistasis. The B-spline model allows for the relationship between the response and predictor variables to be described by a smooth curve.

Owing to sexual dimorphism in our sample (described in more detail in the following paragraphs), we used least squares linear regression to account for the effects of sex on admixture and shape. Because sex ratios varied with Chinese ancestry percentages, it was necessary to adjust both variables to control for the effect of sex entirely. The sex-adjusted residuals were used in all subsequent analyses of the relationship between shape and admixture.

To quantify and visualize the relationship between admixture and pelvic shape, we regressed pelvic shape on admixture using least squares linear regression and then projected the sex-adjusted shape observations onto the resulting regression vector to compute admixture scores (Drake and Klingenberg, 2008; Ledevin and Koyabu, 2019; Sheratt et al., 2019; Moore, 2021). Displayed in a bivariate plot, the results provide a straightforward way to compare the magnitude of shape differences attributable to admixture (the regression trend) to the magnitude of shape differences not explained by the model (residuals about the trend). To visualize the relative contributions of sex and admixture variables to overall shape variation, we display distributions of pairwise Procrustes distances between specimens using different filters of group and sex membership. To test for differences in variance, we used the function morphol.disparity in geomorph (Adams et al., 2020; Collyer and Adams, 2020), which calculates the Procrustes variance for each group, the pairwise distances between group variances, and the *p*-values of tests of significant difference between pairs ($p < 0.05$ throughout).

3. Results

In our intraobserver error analysis, the mean Procrustes distances between iterations of the same individual were much smaller than those between different individuals, and the 95% confidence intervals (CIs) of their means did not overlap. The mean Procrustes distance between iterations of the same individual was 0.026 (95% CI: 0.023–0.029) and 0.036 (95% CI: 0.024–0.048); between different individuals, the mean Procrustes distance was 0.105 (95% CI: 0.101–0.109). We judged this to mean that levels of intraobserver error in our data were within acceptable limits.

3.1. Admixed macaques

As expected, given the known sexual dimorphism in macaque species (e.g., Plavcan, 2001) and the obstetric function of the pelvis, our initial Procrustes ANOVAs showed a relatively high degree of sexual dimorphism in the pelvic morphology of the complete sample: sex explains ~18% of the variation in shape ($F\ [1, 136] = 30.13$, $r^2 = 0.18$, $p < 0.05$). To investigate the nature of sexual dimorphism within the sample, we compared the fit of additive and interaction models of sex and shape (Table 3). The interaction model of the relationship between sex, admixture (% Chinese ancestry), and shape does not fit the data significantly better than a simple additive model, suggesting that sexual dimorphism does not vary with degree of admixture. This being the case, we used additive regression models with sex as the predictor and shape or admixture as the response to produce residuals that allowed us to adjust for sex in both shape and admixture variables for use in further analyses. These residuals are used in all subsequent analyses performed on the complete sample.

After adjusting for sex in both shape and admixture variables, the amount of Chinese ancestry explains a very small, although significant, portion of remaining shape variation: approximately 2% ($F\ [1, 136] = 3.07$, $r^2 = 0.02$, $p < 0.05$). The weak effect of admixture on shape, in contrast to sexual dimorphism, can be seen when pairwise Procrustes distances between the sexes in each Chinese ancestry category are compared with within-sex variation between categories (Fig. 3). Also shown in Figure 3 is variation between members of the same sex within the same admixture category. This can be considered baseline interindividual variation resulting from a combination of many factors, likely including age, weight, and lifetime experiences in the colony. Levels of variation between those with different Chinese ancestry categories, whether adjacent or more distant, are indistinguishable from that baseline variation, demonstrating the very weak effect of admixture compared with other sources of interindividual variation.

The effect of ancestry on pelvic shape (adjusting both for sex) is mostly evident in the shape of the iliac blades (Fig. 4). In animals with more Chinese ancestry, the cranial border of the iliac blades is of relatively equal height, ventral to dorsal, whereas in animals with less Chinese ancestry, the iliac blades extend further laterally and the cranial edges are more angled, extending further cranially at their ventral extent. The dorsal part of the iliac blades, in the region

Table 2
Numbers and definitions of all landmarks (1–48) and semilandmarks (49–204).

Landmark number	Definition
1	Most cranial point on the sacral wing—right
2	Most caudoventral point on the sacral wing, on linea terminalis—right
3	Most lateral point on the cranial articular surface of S1—right
4	Most ventral point on the cranial articular surface of S1 body—midline
5	Most ventral point on the dorsal margin of articular cranial surface of S1 body—midline
6	Most ventral point on the cranial articular surface of S2 body—midline
7	Most caudal point on the sacrum—midline
8	Dorsal caudal iliac spine—right
9	Cranialmost point on the iliac spine—right
10	Cranialmost point on the acetabular rim—right
11	Medialmost point on cranial portion of the lunate—right
12	Medialmost point on caudal portion of the lunate—right
13	Center of the acetabulum—right
14	Caudalmost point on the acetabular rim—right
15	Dorsalmost point on the acetabular rim—right
16	Ventrolateral point on the lateral ischial crest at min. breadth—right
17	Iliac blade medial (most medial intersection of the iliac blade and sacrum)—right
18	Dorsalmost point on the ischial spine—right
19	Intersection of the dorsal ischial crest and ischial tuberosity—right
20	Dorsalmost point on the ischial tuberosity—right
21	Most ventrolateral point on the ischial tuberosity—right
22	Most ventromedial point on the ischial tuberosity—right
23	Cranialmost point on the obturator foramen—right
24	Ventralmost point on the obturator foramen—right
25	Caudalmost point on the obturator foramen—right
26	Pubic symphysis cranial—right
27	Most cranial point on the sacral wing—left
28	Most caudoventral point on the sacral wing, on linea terminalis—left
29	Most lateral point on the cranial articular surface of S1—left
30	Dorsal caudal iliac spine—left
31	Cranialmost point on the iliac spine—left
32	Cranialmost point on the acetabular rim—left
33	Medialmost point on cranial portion of the lunate—left
34	Medialmost point on caudal portion of the lunate—left
35	Center of the acetabulum—left
36	Caudalmost point on the acetabular rim—left
37	Dorsalmost point on the acetabular rim—left
38	Ventrolateral point on the lateral ischial crest at min. breadth—left
39	Iliac crest medial (most medial intersection of the iliac crest and sacrum)—left
40	Dorsalmost point on the ischial spine—left
41	Intersection of the dorsal ischial crest and ischial tuberosity—left
42	Dorsalmost point on the ischial tuberosity—left
43	Most ventrolateral point on the ischial tuberosity—left
44	Most ventromedial point on the ischial tuberosity—left
45	Cranialmost point on the obturator foramen—left
46	Ventralmost point on the obturator foramen—left
47	Most caudodorsal point on the obturator foramen—left
48	Pubic symphysis cranial—left

Semilandmark number	Definition
49 to 88	Pelvic inlet curve
89 to 106	Dorsal ischial curve—right
107 to 124	Dorsal ischial curve—left
125 to 154	Iliac blade curve—right
155 to 184	Iliac blade curve—left
185 to 194	Pubic symphysis curve—right
195 to 204	Pubic symphysis curve—left

Table 3
Comparison (analysis of variance) of interactive and additive models for the relationship between sex, admixture (percent Chinese ancestry), and shape in the complete sample ($n = 138$).

Model	Residual df	df	RSS	SS	r^2	F	p
Shape ~ sex + admix	135	2+	0.508		0.000		
Shape ~ sex * admix	134	3+	0.504	0.004	0.007	1.105	0.292
Total	137		0.635				

The larger interactive model is not a significantly better fit than the smaller additive model.

of the vertebrae S2 and S3 (Fig. 1), also extends more caudally in animals with higher regression scores. There are further differences in the ischium: in higher scoring animals, the medial border of the ischial tuberosities is more laterally placed, compared with animals with lower scores, and the superior border of the pubic symphysis is more ventrally placed. Finally, the sacrum differs between individuals who vary in regression scores: higher scoring individuals have a sacrum that is craniocaudally shorter and more ventrally orientated in the region of S2/S3. All of these differences are very slight, however.

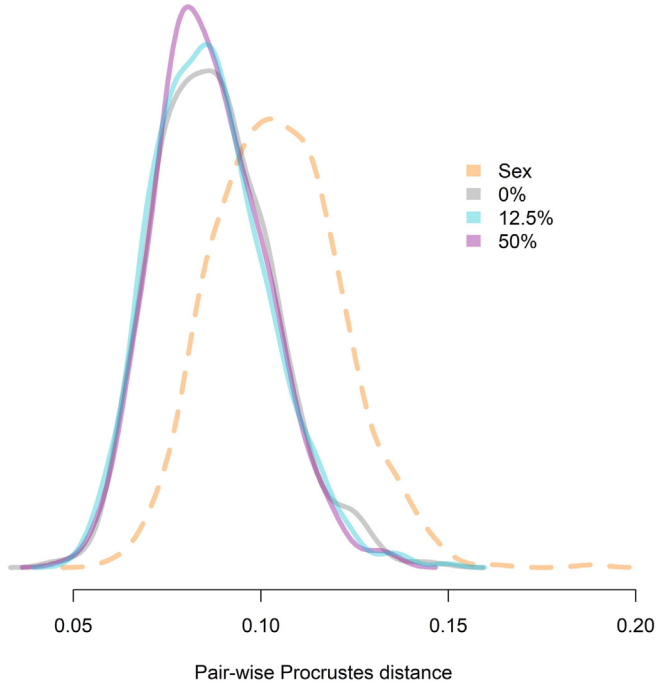

Figure 3. Distributions of pairwise Procrustes distances generated directly from the data. Distributions show distances between members of different sexes within a Chinese ancestry category (orange, dashed line), between individuals of the same sex in the same Chinese ancestry category (gray, solid line), in categories 12.5% apart/adjacent categories (turquoise, solid line), and in categories 50% apart (purple, solid line). Variation between individuals in the same sex and ancestry category (gray, solid line) may be considered baseline levels of variation against which to compare the effects of sex or admixture. (For interpretation of the references to color in this figure legend, the reader is referred to the Web version of this article.)

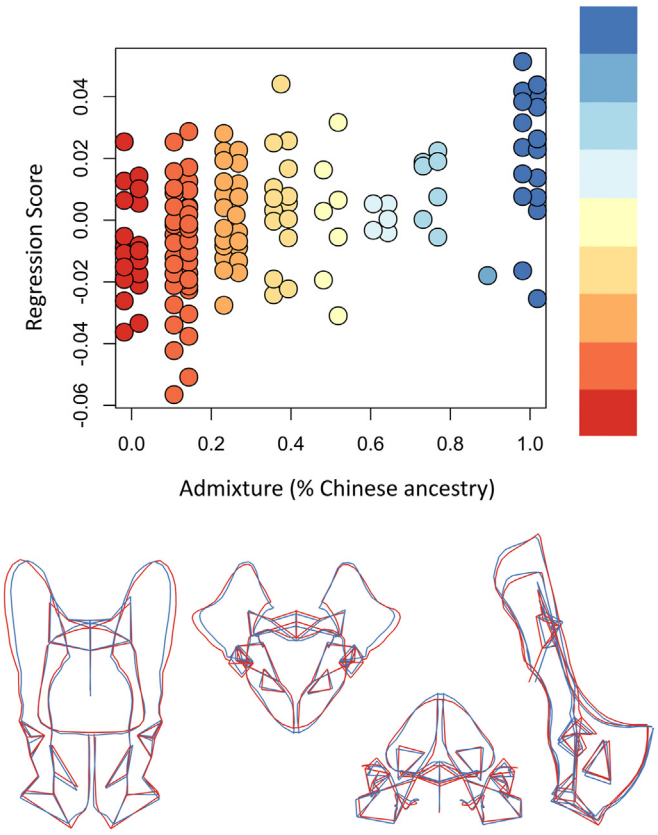

Figure 4. Plot of regression scores showing the relationship between pelvic shape and admixture, both adjusted for sex. Jitter is used to improve the visibility of separate points. Full-bred Indian animals (0% Chinese ancestry) in red; full-bred Chinese animals (100% Chinese ancestry) in dark blue; all other admixture percentages correspond to a color scale between the two extremes, as shown to the right of the graph. Wireframes below the graph show minimum (in red) and maximum (in dark blue) scoring shapes on the regression score axis with displacement magnified by two to aid visualization. Views shown (left to right) are ventral, cranial, caudal, and right lateral. (For interpretation of the references to color in this figure legend, the reader is referred to the Web version of this article.)

The relationship between regression scores and admixture displayed in Figure 4 appears to approach a linear or additive relationship, meaning that change in shape and increasing Chinese ancestry is relatively proportional. This is supported by model comparison, which shows that a three-knot B spline model does not fit the data significantly better than a simple linear model of shape and Chinese ancestry % (adjusted for sex; Table 4).

In the complete sample, there is no significant difference in pelvic centroid size between any pairwise comparison of full-bred Indian, Chinese, or admixed groups (Table 5). Similarly, there are no significant differences between group variances, showing that no one group is more variable in pelvic shape than another (Tables 6 and 7). This suggests there are no transgressive sizes and no increase in shape variation in admixed individuals in this sample.

3.2. Full-bred macaques

In contrast to the full sample analysis (Table 3), analysis of solely the Indian and Chinese full-bred macaques indicates that an interaction model of the relationship between sex and shape is a significantly better fit for the data than an additive model (Table 8). This suggests a difference in sexual dimorphism between the two subspecies that is masked by the greater variation in the complete sample (refer also Clarke and O'Neil, 1999). Owing to these apparent differences in sexual dimorphism, for the full-bred sample we adjusted for differences in the effects of sex on shape separately for each subspecies, by adding the difference between the subspecies-specific male and female means to the female configurations for each subspecies. A PCA showing the separation between the subspecies on the main axes of sex-adjusted shape can be seen in Figure 5. The sex-adjusted residual shapes were used as response variables in a Procrustes ANOVA to quantify the effect of subspecies designation on shape ($F\ [1, 34] = 1.47$, $r^2 = 0.07$, $p < 0.05$). After accounting for sexual dimorphism, there is a significant but fairly weak relationship between the remaining shape variation and subspecies designation (Fig. 6). Designation as Indian or Chinese subspecies accounts for approximately 7% of pelvic shape variation in the full-bred sample.

Figure 6 shows the relationship between regression scores summarizing the proportion of sex-adjusted shape associated with subspecies designation and subspecies designation itself. As with the full sample, there is a difference in pelvic shape associated with Chinese ancestry. Chinese individuals generally have higher regression scores than Indian individuals, showing that they inhabit a different region of the shape space. Compared with the Chinese mean shape, the Indian mean shape is characterized by dorsoventrally and mediolaterally broader iliac blades, which are more angled across the top, running from high ventrally to low dorsally, whereas the tops of the mean Chinese iliac blades are more level. The mean Indian sacrum is more dorsocaudally placed between the ilia, and the sacral alae are shorter craniocaudally. The acetabulae of the mean Indian shape are placed more ventrolaterally, and the pubic symphysis of the mean Indian shape is more dorsally orientated. Finally, the ischial tuberosities of the mean Indian shape extend more caudomedially than those of the mean Chinese shape. These shape differences echo what are seen in

Table 4
Model comparison (analysis of variance) of three-knot B spline and simple additive models for the relationship between shape and admixture in the complete sample ($n = 138$, sex held constant for both variables).

Model	Residual df	df	RSS	SS	r^2	F	*p*
Additive	135	2+	0.508		0.000		
B spline	130	5	0.489	0.120	0.307	1.038	0.388
Total	137		0.635				

The B-spline model is not a significantly better fit than the smaller additive model.

Table 5
Analysis of variance of differences in centroid size between full-bred and admixed animals in the complete sample ($n = 138$).

	df	SS	MS	r^2	F	*P*
Admixture status[a]	2	11377	5688.70	0.04	2.58	0.07[b]
Residuals	135	298013	2207.50	0.96		
Total	137	309391				

[a] Admixture status groups: full-bred Indian, full-bred Chinese, admixed.
[b] There is no significant difference ($p > 0.05$) in centroid size between groups with different admixture status.

Table 6
Procrustes variances for admixture categories in the complete sample ($n = 138$).

Admixture status	Procrustes variance
Ind	0.0043
Chi	0.0049
Ad	0.0046

Ind, full-bred Indian; Chi, full-bred Chinese; Ad, admixed.

Table 7
Test for significant differences in variance (Table 6) between full-bred and admixed animals in the complete sample ($n = 138$).

	Ind	Chi	Ad
Ind	–	0.00054	0.00026
Chi	0.34	–	0.00028
Ad	0.53	0.54	–

Ind, full-bred Indian; Chi, full-bred Chinese; Ad, admixed. Pairwise differences between Procrustes variances are given above the trace; *p*-values of tests of significance of differences are given below the trace. None of the comparisons reaches significance ($p > 0.05$).

Table 8
Comparison (analysis of variance) of additive and interactive models of the relationship between sex, subspecies designation (Indian or Chinese), and shape in the full-bred sample ($n = 36$).

Model	Residual Df	RSS	SS	R^2	F	*p*
Shape ~ sex + subspecies	33	0.149		0.000		
Shape ~ sex * subspecies	32	0.140	0.010	0.059	2.187	0.03
Total	35	0.160				

The interactive model is a significantly better fit than the smaller additive model, as denoted by the significant (<0.05) *p*-value.

Figure 4 and suggest that more Chinese ancestry leads to a pelvis that more closely approaches the mean Chinese shape.

3.3. Projecting admixed individuals onto a vector of full-bred shape

The effect of admixture on sex-adjusted pelvic shape in the complete sample is small, as emphasized by the comparison with baseline interindividual variation within a sex and ancestry category (Fig. 3). Our analyses show, however, that there is a significant

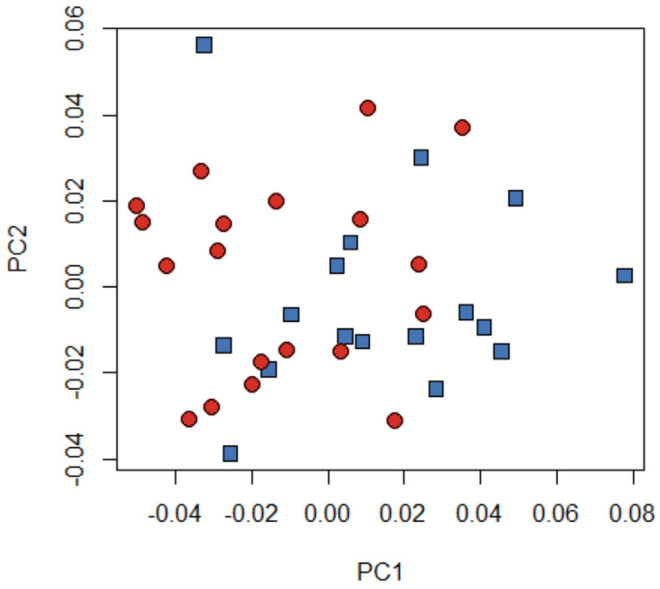

Figure 5. PCA plot showing sex-adjusted shape differences between full-bred species. PC1 accounts for 25.2% variance and PC2 accounts for 13.0% variance. Full-bred Indian animals (0% Chinese ancestry) shown as red circles; full-bred Chinese animals (100% Chinese ancestry) shown as blue squares. This PCA shows the large degree of overlap in pelvic shape between the subspecies on the primary axes of variation. (For interpretation of the references to color in this figure legend, the reader is referred to the Web version of this article.) PCA, principal component analysis.

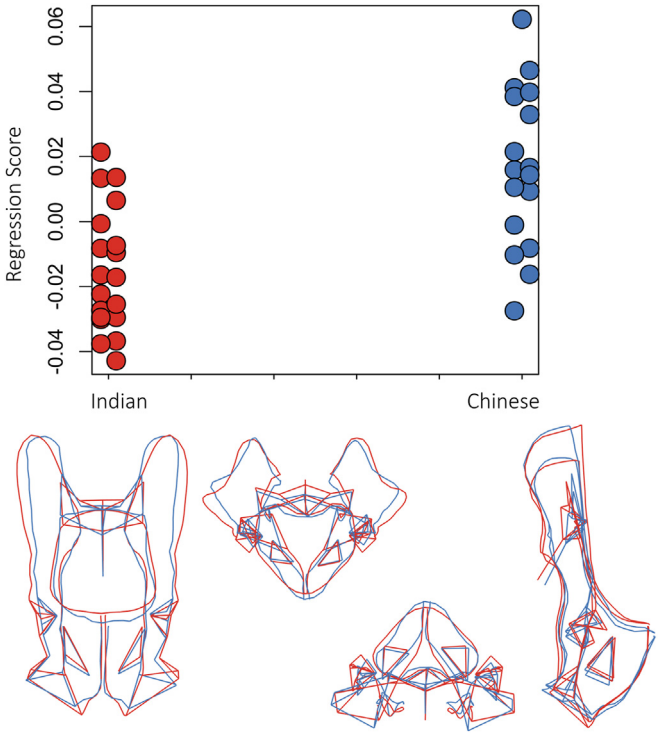

Figure 6. Regression score plot showing the relationship between sex-adjusted shape associated with subspecies designation and subspecies designation. Jitter is used to improve the visibility of separate points. Full-bred Indian (0% Chinese ancestry) animals shown in red; full-bred Chinese (100% Chinese ancestry) animals shown in blue. Wireframes below graph show mean Indian shape (in red) and mean Chinese shape (in blue). Note that this differs from Figure 4, where the wireframes model the extremes of regression scores. As in Figure 4, displacement is magnified by two to aid visualization. Views shown (left to right) are ventral, cranial, caudal, and right lateral. (For interpretation of the references to color in this figure legend, the reader is referred to the Web version of this article.)

relationship between Chinese ancestry and shape and suggest that this is relationship is broadly additive. To examine this possibility further, we created a vector of shape variation using only the sex-adjusted full-bred Indian and Chinese individuals ($n = 36$) and projected the sex-adjusted admixed individuals ($n = 102$) onto this vector (Fig. 7). This figure shows an idealized, linear relationship between Chinese ancestry and sex-adjusted pelvic shape. Comparison of Figures 4 and 7 shows there is very little difference between the modeled relationship and that obtained with the actual data, supporting the assertion that the proportion of Chinese ancestry affects pelvic shape in a predictable, proportional manner.

4. Discussion

The effect of admixture on pelvic shape variation in Indian and Chinese *M. mulatta* is very slight. To put this into context, shape variation between individuals from different Chinese ancestry categories is no greater than intracategory (within sex) variation (Fig. 3). The latter shape variation probably results from multiple variables including age, weight, and stochastic variation. This is in clear contrast to the strong effect of sex on pelvic shape, which cuts across all Chinese ancestry categories.

4.1. The skeletal context

The low levels of pelvic shape differentiation between members of different Chinese ancestry categories are not surprising, given the relatively small differences we found between the full-bred subspecies (Fig. 5). Given the research discussed earlier (see Introduction) suggesting that there are noticeable gross phenotypic differences between Indian and Chinese *M. mulatta* (Clarke and O'Neil, 1999; Fooden, 2000; Hamada et al., 2005), it is possible that the similarity we see in the pelvic data is particular to that region. Skeletal regions display different degrees of canalization and variation (Buck et al., 2010), and the strong selective pressures resulting from the requirements of parturition and locomotion might be expected to lead to stabilizing selection acting on the pelvis. The macaque fit between fetus and birth canal is relatively tight during birth, comparable to that seen in extant humans, and there is evidence in *M. mulatta* of selection on the pelvis to reduce cephalopelvic dystocia (Kawada et al., 2020). The present study is the first analysis of hybrid pelvic morphology. In fact, to the best of our knowledge, it is the first study of any postcranial shape in known hybrids where skeletal shape has been analyzed directly, rather than through the use of proxy measurements taken by palpating bones through soft tissue in live animals (e.g., Kelaita and Cortés-Ortiz, 2013; Fuzessy et al., 2014). Thus, the effects of admixture more widely in human and nonhuman primate pelvic shape remain unknown, and the possibility of regional anatomical differences in admixture signature will be examined in forthcoming work on the crania and other bones from the same sample. If the phenotypic similarity between Chinese and Indian *M. mulatta* is replicated in other regions of the skeleton, these taxa may be relatively phenotypically undifferentiated (skeletally), despite clear genetic differences between them (Zhang and Shi, 1993; Smith and Mcdonough, 2005; Ferguson et al., 2007; Hernandez et al., 2007; Kanthaswamy et al., 2009).

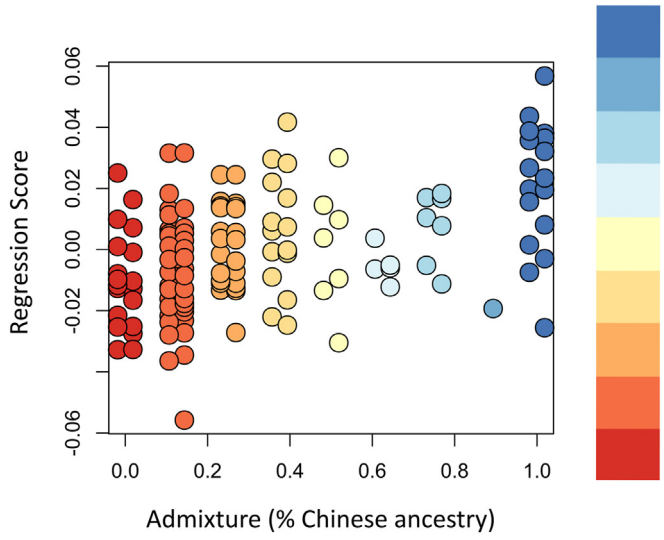

Figure 7. Regression score plot showing the relationship between sex-adjusted shape associated with Chinese ancestry and Chinese ancestry. Shapes of admixed individuals are projected onto a vector constructed using full-bred shape only. Jitter is used to improve the visibility of separate points. Full-bred Indian (0% Chinese ancestry) animals in red; Full-bred Chinese (100% Chinese ancestry) animals in dark blue; all other admixture percentages correspond to a color scale between the two extremes, as shown to the right of the graph. Compare with Figure 4. (For interpretation of the references to color in this figure legend, the reader is referred to the Web version of this article.)

4.2. The macaque context

Morphological research on hybrids between Japanese (*M. fuscata*) and Taiwanese (*M. cyclopis*) macaques shows results comparable with those presented here (Hamada et al., 2012; Ito et al., 2015; Boel et al., 2019). In particular, hybridization between *M. fuscata* and *M. cyclopis* results in a linear correspondence between relative tail length and degree of admixture, with no extreme phenotypes recorded (Hamada et al., 2012), contrary to what is seen for many other nonhuman primate hybrids (refer following paragraphs). *M. fuscata* and *M. cyclopsis* are estimated to have a divergence time of ~170 ka (Chu et al., 2007), close to the ~162 ka estimated for Indian and Chinese *M. mulatta* (Hernandez et al., 2007). GMM-based cranial analyses of these hybrids show no greater levels of variation in hybrids than in parent species and no clear effects of hybrid status on the frequency of anomalous nonmetric traits (Boel et al., 2019). Qualitative comparison of PCAs of the morphospace inhabited by the two full-bred samples, however, does seem to indicate a greater degree of separation between *M. fuscata* and *M. cyclopis* than between the *M. mulatta* subspecies and a tendency of all hybrids toward *M. fuscata* shape, rather than the linear relationship with admixture we describe for our sample (Boel et al., 2019; refer also analysis of linear measurements in; Ito et al., 2015). The Japanese-Taiwanese hybrids were wild caught in Japan (Ito et al., 2015; Boel et al., 2019), at a higher latitude and in a more temperate climate than Taiwan. Therefore, there may be some adaptive advantage in *M. fuscata* morphology leading to the dominance of *M. fuscata*-like morphology in hybrids and also potentially selection for greater phenotypic divergence between the parent taxa after their separation in the Pleistocene, if their habitats are less similar than those of Indian and Chinese *M. mulatta*.

4.3. The nonhuman primate context

In contrast to much of the previous research on nonhuman primates (Ackermann et al., 2006, 2014; Kelaita and Cortés-Ortiz, 2013; Fuzessy et al., 2014) with the exception of other macaque studies (refer previous paragraphs), in this study, we found no increased shape variation and no heterosis or transgressive size in the hybrid sample. There are several possible factors that may contribute to this difference from earlier work, including the

methods used, the range of admixture of the hybrids making up each sample and the degree of similarity (phenotypic or genetic) between the parent taxa in each study.

In the present study, we used landmark-based GMM to compare overall pelvic shape, while by contrast, most studies of hybrid morphology in nonhuman primates (e.g., Ackermann et al., 2006, 2014; Kelaita and Cortés-Ortiz, 2013; Fuzessy et al., 2014; Ito et al., 2015) have used traditional morphometrics and nonmetric traits. This may, in part, account for differences in results between studies, as analysis of individual nonmetric traits or measurements can emphasize greater difference between specific regions that may be averaged out by analyses of overall shape using GMM. Similar GMM used to analyze shape in hybrid mouse crania show patterns of increased variation and extreme phenotypes similar to those seen in baboons (Warren et al., 2018), however, suggesting that GMM is not entirely responsible for the differences in results between studies.

Hybridization in the baboon colony studied by Ackermann et al. (2006, 2014) was only a few generations deep, and many transgressive or anomalous morphologies characterized as the products of hybridization are most likely to occur in the F1 generation or in generations close to the interbreeding event (Prentis et al., 2008). This likely contributes to our lack of such a signal in the current sample, which contains fewer early generation hybrids and only one F1 individual. More subtle manifestations of expected hybrid morphology, however, such as some individuals of transgressive size/shape and greater variation within admixed samples, have also been documented in naturally hybridizing populations of marmosets and howler monkeys, where far fewer individuals are likely to be early generation hybrids (Kelaita and Cortés-Ortiz, 2013; Fuzessy et al., 2014). This suggests that the admixture proportions sampled here may not completely explain the more linear relationship between admixture and pelvic morphology in our results.

A final possible reason for the novelty of our results, in relation to the majority of nonhuman primate hybrid research, may be relatively short divergence time between the *M. mulatta* parent taxa compared with the parent taxa investigated in previous work. Baboon taxonomy is much debated, but a recent article by Rogers et al. (2019) suggests that the lineages of the olive and yellow baboon allotaxa studied by Ackermann and colleagues (Ackermann et al., 2006, 2014) diverged about 1.4 Ma. Black (*Alouatta pigra*) and mantled (*A. palliata*) howler monkeys, as studied by Kelaita and Cortés-Ortiz (2013), are still more phylogenetically divergent, with a split time of ~3 Ma (Cortés-Ortiz et al., 2003), while *Callithrix* is a fairly young genus and the black-tufted and white-headed marmosets (*C. penicillata* and *C. geoffroyi*, respectively), whose hybrids have been studied by Fuzessy et al. (2014), split ~700 ka (Malukiewicz et al., 2017). Based on these dates, the genetic distance between Indian and Chinese *M. mulatta*, estimated to have diverged ~162 ka (Hernandez et al., 2007), is considerably less than that between these other taxa. There also remains the possibility that the rhesus macaques are less differentiated morphologically relative to their genetic distance, perhaps due to stabilizing selection (refer also to section 4.4). This is an interesting possibility, which has not yet been investigated and which should be followed up by the comparison of further nonhuman primate taxa pairs with similar phylogenetic divergence times.

The differences between results presented here and previous work on nonhuman primate hybrids, as well as between previous studies, demonstrate the complex relationship between taxonomic divergence and hybrid morphology, which is not yet fully understood. Similarly, these differences indicate the need for further investigation to better understand which nonhuman primate species make the best models for hominin hybridization. It has been shown that more genetically divergent taxa lead to more transgressive hybrids, due to increasing fixation of different alleles in each parent taxon over time (i.e., fixed differences in alleles as opposed to differences in allele frequencies), which may lead to complementary gene action or epistasis in hybrid offspring (Stelkens and Seehausen, 2009; Stelkens et al., 2009; Comeault and Matute, 2018; Allen et al., 2020). The relationship between phenotypic divergence and transgressive phenotypes is less clear, however (Stelkens and Seehausen, 2009; Stelkens et al., 2009), and relationships among divergence time and genetic and phenotypic differentiation appear to differ between groups of organisms (Stelkens and Seehausen, 2009; McGee et al., 2016). Most vertebrate research on these relationships to date has been in fish (Stelkens and Seehausen, 2009; Stelkens et al., 2009; McGee et al., 2016). Thus, it is also unclear how well these results translate to primates, making this area ripe for further investigation.

4.4. The paleoanthropological context

From a paleoanthropological point of view, it is relevant that there appears to be considerably less variation in pelvic shape between Indian and Chinese *M. mulatta* than between Neanderthals and *H. sapiens*, a hybridizing taxon pair with reasonably comparable levels of genetic relatedness (see Introduction). Further examination of other aspects of the *M. mulatta* skeleton and other pairs of nonhuman primate taxa will be required to determine whether, given their genetic distance, Indian and Chinese rhesus macaques are relatively phenotypically similar or whether *H. sapiens* and Neanderthals are more divergent than would be expected within the context of the primate order. If shown to be present throughout the skeleton, low levels of phenotypic differentiation between Chinese and Indian *M. mulatta* might suggest stabilizing selection, while the mechanism leading to relatively high differentiation between the hominin taxa could be either directional selection or neutral evolution. If stabilizing selection has played a lesser role in the evolutionary history of the hominin pelvis than that of macaques, this could reflect a wider trend. For example, Schroeder and von Cramon Taubadel (2017) have shown that across all sampled extant hominoid taxa, hominoid cranial evolution is characterized by stabilizing selection with very few exceptions, one of which is marked directional selection in the hominin lineage after its split with the chimpanzee lineage. The pelvic evidence from the present study may suggest that this pattern holds throughout the skeleton. The presence of unusually high levels of phenotypic differentiation in hominins (Lynch, 1990) is supported by comparison of rates of cranial evolution in the *Pan* clade versus the Neanderthal/*H. sapiens* clade (Weaver, 2014) and by comparisons between Neanderthal/*H. sapiens* morphological divergence and that between other catarrhine pairs (Harvati et al., 2004). It has been suggested that a unique human ecological niche, typified by cultural adaptation, has allowed the build-up of uncommonly great neutral variation in our lineage due to reduced selection (including stabilizing selection) compared with other organisms (Ackermann and Cheverud, 2004; Wells and Stock, 2007; Weaver and Stringer, 2015; Buck et al., 2019).

There is, however, also a strong argument for selection leading to greater pelvic variation between *H. sapiens* and Neanderthals than between Indian and Chinese *M. mulatta*. Indian- and Chinese-derived *M. mulatta* are likely phenotypically similar, at least in part because they have inhabited similar habitats since their divergence

(Hamada et al., 2005). This is in contrast to *H. sapiens* and Neanderthals, which adapted for hundreds of thousands of years to the disparate climates and habitats of Africa and Western Eurasia, respectively (Holliday, 1997a, b). Climate has played a role in extant human pelvic shape variation (Betti et al., 2014), and it is also thought to have affected pelvic morphology in extinct hominins (Ruff, 1993; Weaver, 2009). In addition to, or as an alternative to the effects of climate, directional selection leading to cranial vault expansion in the hominin lineage, as reported by Schroeder and von Cramon Taubadel (2017), could play a role in pelvic change via the requirement for congruence during parturition. If this is the case, the simultaneous cranial expansion but divergent cranial shapes in the *H. sapiens* and Neanderthal lineages could have contributed to their differences in pelvic morphology.

The seeds of relatively great divergence in pelvic shape between hominin species may lie still deeper in hominin evolution. It has been suggested that integration has been relaxed in the human pelvis relative to other hominids, allowing for greater evolvability and selection for bipedal morphology (Grabowski et al., 2011). This possibility is borne out by the high levels of intraspecific geographic variation in human pelvic morphology compared with other skeletal regions (Betti and Manica, 2018). A breakdown in integration is likely governed by changes to the underlying genetic architecture controlling pelvic development and evidence that distinctive hominin pelvis shape results from a unique growth trajectory emerging relatively early in development also suggests modification of genetically determined pathways (Zirkle and Lovejoy, 2019). Different genetic underpinning and levels of integration in macaques and hominins could mean that similar degrees of genetic difference could affect phenotypic outcomes in different ways. This scenario could facilitate the potential development of adaptive differences in one group (e.g., Neanderthals/*H. sapiens*) but neutral divergence in the other (e.g., Indian/Chinese *M. mulatta*). We note that the possibilities of directional selection and unusually high neutral variation are not mutually exclusive and could have combined to produce particularly phenotypically divergent taxa in *H. sapiens* and Neanderthals.

One could argue that, owing to their lower levels of phenotypic disparity relative to the time depth of their divergence, Indian/Chinese *M. mulatta* pelves are not a good model for the phenotypic effects of hybridization in hominins. It may, however, be difficult to find a pair of primate taxa with a similar divergence time to *H. sapiens*/Neanderthals and similar morphological disparity, highlighting the peculiarity of these hominin sister taxa. Most of the taxon pairs in the nonhuman primate hybrid literature have greater phylogenetic split times, and, although there is no way of directly comparing parent taxon phenotypic disparity between studies, the stronger admixture effects seen in previous studies may in part be related to greater phenotypic differentiation between parent taxa (see section 4.3).

Although weak, the linear nature of the relationship between admixture and pelvic shape we find here is nonetheless informative. Greater Chinese ancestry leads to a pelvic shape which is closer to the mean shape for full-bred Chinese individuals, and the difference in Chinese ancestry is proportional to the difference in pelvic shape. If further investigation bears out the suggestion of the results we present here—that the morphology of hybrids between closely related primate taxa is proportional to the input of each parent taxon—this information can be used to further investigate the expected morphology of hominin hybrids. Models of expected hominin hybrid morphology can be constructed with the known morphology of parent taxa; for example, Neanderthal and *H. sapiens* crania as the endpoints of the hypothetical shape vector along which all admixed individuals would fall. Thus, the magnitude of disparity between parental shapes would not affect the pattern of the hybrids that fall between them, if the pattern of variation is a valid analog.

5. Conclusions

From a large sample of multigenerational hybrids and full-bred Indian and Chinese *M. mulatta*, we find the effects of admixture on pelvic shape to be very small, albeit significant, comparable with interindividual differences between members of the same sex and admixture category. The admixture signal we identify is linear, with greater Chinese ancestry resulting in a pelvic shape that more closely approximates that of full-bred Chinese *M. mulatta*. We find no evidence for an increase in size or shape variation nor transgressive morphologies in hybrids. Taken in the context of the existing nonhuman primate hybrid literature, the small effect and additive nature of the admixture signal in *M. mulatta* pelvic shape is likely affected by a combination of factors, including the phylogenetic closeness of the parent taxa relative to that between previously studied taxon pairs (Ackermann et al., 2006, 2014; Kelaita and Cortés-Ortiz, 2013; Fuzessy et al., 2014), the similarity of Indian and Chinese *M. mulatta* habitat and ecological niche since their divergence (Hamada et al., 2005), and the low number of early generation hybrids in the present study. Despite the interesting disparity in phenotypic divergence between the Indian and Chinese *M. mulatta* and Neanderthals/*H. sapiens*, which deserves further investigation, the relative similarity in phylogenetic closeness (refer also Allen et al., 2020) and the multiple generations of hybridization in the current sample of *M. mulatta* have resulted in a useful analog for hominin hybridization. Models of hypothetical outcomes of hybridization between Neanderthals and *H. sapiens*, using the pattern revealed by these *M. mulatta* results, can now be tested against the fossil record to increase our understanding of the impacts of interbreeding on human evolution.

Conflict of interest statement

The authors declare no conflict of interest.

Acknowledgments

This research was funded by the National Science Foundation (BCS 1623366, 1720128) and the Leakey Foundation, with further support to R.R.A. from the National Research Foundation of South Africa. The authors thank the Editor, Associate Editor, and three anonymous reviewers for their constructive comments, which have much improved this article. The authors thank Mark Grote for his substantial statistical assistance. The authors are grateful to CNPRC staff, including Alice Tarantal for overseeing CT scanning, and Paul-Michael Sosa, Daniel Quiros Molina, Jennifer Short, and Sarah Davis for their extensive help with data collection. The authors thank Irene Englis and staff at the University of California Davis Museum of Wildlife and Fish Biology, for skeletonizing remains involved in this study. L.T.B. is grateful to Alex Cantó Pastor, Austin Reynolds, Mark Grabowski, Aurélien Mounier, and Florent Détroit for help with coding, and the authors thank Amber Parks and Sara Jhanjar for all their help with segmenting CT scans.

Supplementary Online Material

Supplementary online material to this article can be found online at https://doi.org/10.1016/j.jhevol.2021.103049.

References

Ackermann, R.R., Arnold, M.L., Baiz, M.D., Cahill, J.A., Cortés-Ortiz, L., Evans, B.J., Grant, B.R., Grant, P.R., Hallgrimsson, B., Humphreys, R.A., Jolly, C.J.,

Malukiewicz, J., Percival, C.J., Ritzman, T.B., Roos, C., Roseman, C.C., Schroeder, L., Smith, F.H., Warren, K.A., Wayne, R.K., Zinner, D., 2019. Hybridization in human evolution: insights from other organisms. Evol. Anthropol. 28, 189–209.
Ackermann, R.R., Bishop, J.M., 2010. Morphological and molecular evidence reveals recent hybridization between gorilla taxa. Evolution 64, 271–290.
Ackermann, R.R., Cheverud, J.M., 2004. Detecting genetic drift versus selection in human evolution. Proc. Natl. Acad. Sci. USA 101, 17946–17951.
Ackermann, R.R., Mackay, A., Arnold, M.L., 2016. The hybrid origin of "Modern" Humans. Evol. Biol. 43, 1–11.
Ackermann, R.R., Rogers, J., Cheverud, J.M., 2006. Identifying the morphological signatures of hybridization in primate and human evolution. J. Hum. Evol. 51, 632–645.
Ackermann, R.R., Schroeder, L., Rogers, J., Cheverud, J.M., 2014. Further evidence for phenotypic signatures of hybridization in descendent baboon populations. J. Hum. Evol. 76, 54–62.
Adams, D.C., Collyer, M.L., Kaliontzopoulou, A., 2020. Geomorph: Software for geometric morphometric analyses, Ver. 3.2.1. https://cran.r-project.org/package=geomorph.
Allen, R., Ryan, H., Davis, B.W., King, C., Frantz, L., Irving-pease, E., Barnett, R., Linderholm, A., Loog, L., Haile, J., Lebrasseur, O., White, M., Kitchener, A.C., Murphy, W.J., Larson, G., Murphy, W.J., 2020. A mitochondrial genetic divergence proxy predicts the reproductive compatibility of mammalian hybrids. Proc. Royal Soc. B Biol. Sci. 287, 20200690.
Bergmann, C.A., 1847. Uber die Verhaltnisee der Warmeokonomie der Thiere zu iher Grosse, vol. 1. Gottingen Studien, pp. 595–708.
Betti, L., Manica, A., 2018. Human variation in the shape of the birth canal is significant and geographically structured. Proc. Royal Soc. B Biol. Sci. 285, 20181807.
Betti, L., von Cramon-Taubadel, N., Manica, A., Lycett, S.J., 2014. The interaction of neutral evolutionary processes with climatically-driven adaptive changes in the 3D shape of the human os coxae. J. Hum. Evol. 73, 64–74.
Bocquet-Appel, J.P., Degioanni, A., 2013. Neanderthal demographic estimates. Curr. Anthropol. 54, S202–S213.
Boel, C., Curnoe, D., Hamada, Y., 2019. Craniofacial shape and nonmetric trait variation in hybrids of the Japanese macaque (*Macaca fuscata*) and the Taiwanese macaque (*Macaca cyclopis*). Int. J. Primatol. 40, 214–243.
Buck, L.T., De Groote, I., Hamada, Y., Hassett, B.R., Ito, T., Stock, J.T., 2019. Evidence of different climatic adaptation strategies in humans and non-human primates. Sci. Rep. 9, 11025.
Buck, L.T., Stock, J.T., Foley, R.a., 2010. Levels of intraspecific variation within the catarrhine skeleton. Int. J. Primatol. 31, 779–795.
Chu, J.H., Lin, Y.S., Wu, H.Y., 2007. Evolution and dispersal of three closely related macaque species, *Macaca mulatta, M. cyclopis*, and *M. fuscata*, in the eastern Asia. Mol. Phylogenet. Evol. 43, 418–429.
Clarke, M.R., O'Neil, J.A.S., 1999. Morphometric comparison of Chinese-origin and Indian-derived rhesus monkeys (*Macaca mulatta*). Am. J. Primatol. 74, 335–346.
Collyer, M.L., Adams, D.C., 2018. RRPP: An R package for fitting linear models to high-dimensional data using residual randomization. Methods Ecol. Evol. 9, 1772–1779.
Collyer, M.L., Adams, D.C., 2020. RRPP: Linear model evaluation and randomized residuals in a permutation procedure, Ver. 0.5.2. https://cran.r-project.org/package=RRPP.
Comeault, A.A., Matute, D.R., 2018. Genetic divergence and the number of hybridizing species affect the path to homoploid hybrid speciation. Proc. Natl. Acad. Sci. USA 115, 9761–9766.
Cortés-Ortiz, L., Bermingham, E., Rico, C., Rodríguez-Luna, E., Sampaio, I., Ruiz-García, M., 2003. Molecular systematics and biogeography of the Neotropical monkey genus, *Alouatta*. Mol. Phylogenet. Evol. 26, 64–81.
Cortés-Ortiz, L., Roos, C., Zinner, D., 2019. Introduction to special issue on primate hybridization and hybrid zones. Int. J. Primatol. 40, 1–8.
Drake, A.G., Klingenberg, C.P., 2008. The pace of morphological change: Historical transformation of skull shape in St. Bernard dogs. Proc. Royal Soc. B Biol. Sci. 275, 71–76.
Duarte, C., Maurício, J., Pettitt, P.B., Souto, P., Trinkaus, E., Van Der Plicht, H., Zilhão, J., 1999. The early Upper Paleolithic human skeleton from the Abrigo do Lagar Velho (Portugal) and modern human emergence in Iberia. Proc. Natl. Acad. Sci. USA 96, 7604–7609.
Ferguson, B., Street, S.L., Wright, H., Pearson, C., Jia, Y., Thompson, S.L., Allibone, P., Dubay, C.J., Spindel, E., Norgren, R.B., 2007. Single nucleotide polymorphisms (SNPs) distinguish Indian-origin and Chinese-origin rhesus macaques (*Macaca mulatta*). BMC Genom. 8, 43.
Fischer, J., Higham, J.P., Alberts, S.C., Barrett, L., Beehner, J.C., Bergman, T.J., Carter, A.J., Collins, A., Elton, S., Fagot, J., Ferreira da Silva, M.J., Hammerschmidt, K., Henzi, P., Jolly, C.J., Knauf, S., Kopp, G.H., Rogers, J., Roos, C., Ross, C., Seyfarth, R.M., Silk, J., Snyder-Mackler, N., Staedele, V., Swedell, L., Wilson, M.L., Zinner, D., 2019. The natural history of model organisms: Insights into the evolution of social systems and species from baboon studies. eLife 8, e50989.
Fooden, J., 1976. Provisional classification and key to living species of macaques (Primates: *Macaca*). Folia Primatol. 25, 225–236.
Fooden, J., 1982. Ecogeographic segregation of macaque species. Primates 23, 574–579.
Fooden, J., 1995. Systematic review of Southeast Asian longtail macaques, *Macaca fascicularis* (Raffles, 1821). Fieldiana Zool. 81, 2–3.
Fooden, J., 2000. Zoology Systematic Review of the Rhesus Macaque, *Macaca mulatta* (Zimmermann, 1780). Field Museum of Natural History, Chicago.
Fooden, J., 2006. Comparative review of *fascicularis*-group species of macaques (Primates: *Macaca*). Fieldiana Zool. 107, 1–43.
Fu, Q., Hajdinjak, M., Moldovan, O.T., Constantin, S., Mallick, S., Skoglund, P., Patterson, N., Rohland, N., Lazaridis, I., Nickel, B., Viola, B., Prüfer, K., Meyer, M., Kelso, J., Reich, D., Pääbo, S., 2015. An early modern human from Romania with a recent Neanderthal ancestor. Nature 524, 216–219.
Fuzessy, L.F., Silva, I. de O., Malukiewicz, J., Silva, F.F.R., Pônzio, M. do C., Boere, V., Ackermann, R.R., 2014. Morphological variation in wild marmosets (*Callithrix penicillata* and *C. geoffroyi*) and their hybrids. Evol. Biol. 41, 480–493.
Gopalan, S., Atkinson, E.G., Buck, L.T., Weaver, T.D., Henn, B.M., 2021. Inferring archaic introgression from hominin genetic data. Evol. Anthropol. 30, 199–220.
Grabowski, M.W., Polk, J.D., Roseman, C.C., 2011. Divergent patterns of integration and reduced constraint in the human hip and the origins of bipedalism. Evolution 65, 1336–1356.
Green, R.E., Krause, J., Briggs, A.W., Maricic, T., Stenzel, U., Kircher, M., Patterson, N., Li, H., Zhai, W., Fritz, M.H.-Y., Hansen, N.F., Durand, E.Y., Malaspinas, A.-S., Jensen, J.D., Marques-Bonet, T., Alkan, C., Prüfer, K., Meyer, M., Burbano, H.A., Good, J.M., Schultz, R., Aximu-Petri, A., Butthof, A., Höber, B., Höffner, B., Siegemund, M., Weihmann, A., Nusbaum, C., Lander, E.S., Russ, C., Novod, N., Affourtit, J., Egholm, M., Verna, C., Rudan, P., Brajkovic, D., Kucan, Z., Gusic, I., Doronichev, V.B., Golovanova, L.V., Lalueza-Fox, C., de la Rasilla, M., Fortea, J., Rosas, A., Schmitz, R.W., Johnson, P.L.F., Eichler, E.E., Falush, D., Birney, E., Mullikin, J.C., Slatkin, M., Nielsen, R., Kelso, J., Lachmann, M., Reich, D., Pääbo, S., 2010. A draft sequence of the Neandertal genome. Science 328, 710–722.
Gunz, P., Neubauer, S., Golovanova, L., Doronichev, V., Maureille, B., Hublin, J.J., 2012. A uniquely modern human pattern of endocranial development. Insights from a new cranial reconstruction of the Neandertal newborn from Mezmaiskaya. J. Hum. Evol. 62, 300–313.
Hamada, Y., Watanabe, T., Chatani, K., Hayakawa, S., Iwamoto, M., 2005. Morphometrical comparison between Indian- and Chinese-derived rhesus macaques (*Macaca mulatta*). Anthropol. Sci. 113, 183–188.
Hamada, Y., Yamamoto, A., Kunimatsu, Y., Tojima, S., Mouri, T., Kawamoto, Y., 2012. Variability of tail length in hybrids of the Japanese macaque (*Macaca fuscata*) and the Taiwanese macaque (*Macaca cyclopis*). Primates 53, 397–411.
Harvati, K., Frost, S.R., McNulty, K.P., 2004. Neanderthal taxonomy reconsidered: implications of 3D primate models of intra- and interspecific differences. Proc. Natl. Acad. Sci. USA 101, 1147–1152.
Hayasaka, K., Fujii, K., Horai, S., 1996. Molecular phylogeny of macaques: Implications of nucleotide sequences from an 896-base pair region of mitochondrial DNA. Mol. Biol. Evol. 13, 1044–1053.
Hernandez, R.D., Hubisz, M.J., Wheeler, D.A., Smith, D.G., Ferguson, B., Rogers, J., Nazareth, L., Indap, A., Bourquin, T., McPherson, J., Muzny, D., Gibbs, R., Nielsen, R., Bustamante, C.D., 2007. Demographic histories and patterns of linkage disequilibrium in Chinese and Indian rhesus macaques. Science 316, 240–243.
Holliday, T.W., 1997a. Postcranial evidence of cold adaptation in European Neandertals. Am. J. Phys. Anthropol. 104, 245–258.
Holliday, T.W., 1997b. Body proportions in Late Pleistocene Europe and modern human origins. J. Hum. Evol. 32, 423–448.
Ito, T., Kawamoto, Y., Hamada, Y., Nishimura, T.D., 2015. Maxillary sinus variation in hybrid macaques: Implications for the genetic basis of craniofacial pneumatization. Biol. J. Linn. Soc. 115, 333–347.
Jolly, C.J., 2001. A proper study for mankind: analogies from the papionin monkeys and their implications for human evolution. Am. J. Phys. Anthropol. 116, 177–204.
Kanthaswamy, S., Gill, L., Satkoski, J., Goyal, V., Malladi, V., Kou, A., Basuta, K., Sarkisyan, L., George, D., Smith, D.G., 2009. Development of a Chinese-Indian hybrid (Chindian) rhesus macaque colony at the California National primate research center by introgression. J. Med. Primatol. 38, 86–96.
Kawada, M., Nakatsukasa, M., Nishimura, T., Kaneko, A., Morimoto, N., 2020. Covariation of fetal skull and maternal pelvis during the perinatal period in rhesus macaques and evolution of childbirth in primates. Proc. Natl. Acad. Sci. USA 117, 202002112.
Kelaita, M.A., Cortés-Ortiz, L., 2013. Morphological variation of genetically confirmed *Alouatta pigra* × *A. palliata* hybrids from a natural hybrid zone in Tabasco, Mexico. Am. J. Phys. Anthropol. 150, 223–234.
Ledevin, R., Koyabu, D., 2019. Patterns and constraints of craniofacial variation in colobine monkeys: Disentangling the effects of phylogeny, allometry and diet. Evol. Biol. 46, 14–34.
Lynch, M., 1990. The rate of morphological evolution in mammals from the standpoint of the neutral expectation. Am. Nat. 136, 727–741.
Malukiewicz, J., Hepp, C.M., Guschanski, K., Stone, A.C., 2017. Phylogeny of the *jacchus* group of *Callithrix* marmosets based on complete mitochondrial genomes. Am. J. Phys. Anthropol. 162, 157–169.
Martinez, F.I., Capelli, C., Ferreira da Silva, M.J., Aldeias, V., Alemseged, Z., Archer, W., Bamford, M., Biro, D., Bobe, R., Braun, D.R., Habermann, J.M., Lüdecke, T., Madiquida, H., Mathe, J., Negash, E., Paulo, L.M., Pinto, M., Stalmans, M., Tátá, F., Carvalho, S., 2019. A missing piece of the *Papio* puzzle: Gorongosa baboon phenostructure and intrageneric relationships. J. Hum. Evol. 130, 1–20.
McGee, M.D., Neches, R.Y., Seehausen, O., 2016. Evaluating genomic divergence and parallelism in replicate ecomorphs from young and old cichlid adaptive radiations. Mol. Ecol. 25, 260–268.

Melnick, D.J., Hoelzer, G.a, Absher, R., Ashley, M.V., 1993. mtDNA diversity in rhesus monkeys reveals overestimates of divergence time and paraphyly with neighboring species. Mol. Biol. Evol. 10, 282–295.
Meyer, M., Arsuaga, J.L., de Filippo, C., Nagel, S., Aximu-Petri, A., Nickle, B., Martínez, I., Gracia, A., de Castro, J.M.B., Carbonell, E., Viola, B., 2016. Nuclear DNA sequences from the Middle Pleistocene Sima de los Huesos hominins. Nature 531, 504–507.
Mitteroecker, P., Huttegger, S.M., Fischer, B., Pavlicev, M., 2016. Cliff-edge model of obstetric selection in humans. Proc. Natl. Acad. Sci. USA 113, 14680–14685.
Mitteroecker, P., Windhager, S., Pavlicev, M., 2017. Cliff-edge model predicts intergenerational predisposition to dystocia and Caesarean delivery. Proc. Natl. Acad. Sci. USA 114, 11669–11672.
Moore, A.J., 2021. Vertebral pneumaticity is correlated with serial variation in vertebral shape in storks. J. Anat. 238, 615–625.
Moorjani, P., Sankararaman, S., Fu, Q., Przeworski, M., Patterson, N., Reich, D., 2016. A genetic method for dating ancient genomes provides a direct estimate of human generation interval in the last 45,000 years. Proc. Natl. Acad. Sci. USA 113, 5652–5657.
Plavcan, J.M., 2001. Sexual dimorphism in primate evolution. Yearb. Phys. Anthropol. 44, 25–53.
Ponce de León, M.S., Zollikofer, C.P.E., 2001. Neanderthal cranial ontogeny and its implications for late hominid diversity. Nature 412, 534–538.
Prentis, P.J., Wilson, J.R.U., Dormontt, E.E., Richardson, D.M., Lowe, A.J., 2008. Adaptive evolution in invasive species. Trends Plant Sci. 13, 288–294.
R Core Team, 2018. R: A Language and Environment for Statistical Computing. R Foundation for Statistical Computing, Vienna, Austria.
Rak, Y., Arensburg, B., 1987. Kebara 2 Neanderthal pelvis: first look at a complete inlet. Am. J. Phys. Anthropol. 73, 227–231.
Rogers, J., Raveendran, M., Harris, R.A., Mailund, T., Leppälä, K., Athanasiadis, G., Schierup, M.H., Cheng, J., Munch, K., Walker, J.A., Konkel, M.K., Jordan, V.E., Steely, C.J., Beckstrom, T.O., Bergey, C., Burrell, A., Schrempf, D., Noll, A., Kothe, M., Kopp, G.H., Liu, Y., Murali, S., Billis, K., Martin, F.J., Muffato, M., Cox, L.A., Else, J., Disotell, T., Muzny, D.M., Phillips-Conroy, J., Aken, B., Eichler, E.E., Marques-Bonet, T., Kosiol, C., Batzer, M.A., Hahn, M.W., Tung, J., Zinner, D., Roos, C., Jolly, C.J., Gibbs, R.A., Worley, K.C., Archidiacono, N., Capozzi, O., Catacchio, C.R., Dinh, H.H., Doddapaneni, H.V., Han, Y., Huddleston, J., Jhangiani, S.N., Karimpour-Fard, A., Korchina, V., Kovar, C.L., Kuderna, L., Lee, S.L., Liu, X., Marra-Campanale, A., Mason, C.E., Montero, M. de M., Pagel, K.A., Palazzo, A., Pecotte, J., Pejaver, V., Pipes, L., Quick, V.S., Radivojac, P., Raja, A., Raney, B.J., Rice, K., Rocchi, M., Sikela, J.M., Stanyon, R., Thomas, G.W.C., Ventura, M., Vilgalys, T.P., Vinar, T., Walter, L., 2019. The comparative genomics and complex population history of *Papio* baboons. Sci. Adv. 5, eaau6947.
Rougier, H., Milota, Ş., Rodrigo, R., Gherase, M., Sarcină, L., Moldovan, O., Zilhão, J., Constantin, S., Franciscus, R.G., Zollikofer, C.P.E., De León, M.P., Trinkaus, E., 2007. Peştera cu Oase 2 and the cranial morphology of early modern Europeans. Proc. Natl. Acad. Sci. USA 104, 1165–1170.
Ruff, C., 1993. Climatic adaptation and hominid evolution: the thermoregulatory imperative. Evol. Anthropol. 2, 53–60.
Sankararaman, S., Patterson, N., Li, H., Pääbo, S., Reich, D., 2012. The date of interbreeding between Neandertals and modern humans. PLoS Genet. 8, e1002947.
Savriama, Y., Valtonen, M., Kammonen, J.I., Rastas, P., Smolander, O.P., Lyyski, A., Häkkinen, T.J., Corfe, I.J., Gerber, S., Salazar-Ciudad, I., Paulin, L., Holm, L., Löytynoja, A., Auvinen, P., Jernvall, J., 2018. Bracketing phenogenotypic limits of mammalian hybridization. Roy. Soc. Open Sci. 5, 180903.
Schlager, S., 2017. Morpho and Rvcg - shape analysis in R. In: Zheng, G., Li, S., Szekely, G. (Eds.), Statistical Shape and Deformation Analysis. Academic Press, Cambridge, pp. 217–256.
Schroeder, L., von Cramon-Taubadel, N., 2017. The evolution of hominoid cranial diversity: A quantitative genetic approach. Evolution 71, 2634–2649.
Sheratt, E., Sanders, K.L., Watson, A., Hutchinson, M.N., Lee, M.S., Palci, A., 2019. Heterochronic shifts mediate ecomorphological convergence in skull shape of microcephalic sea snakes. Integr. Comp. Biol. 59, 616–624.
Smith, D.G., Mcdonough, J., 2005. Mitochondrial DNA variation in Chinese and Indian Rhesus macaques (*Macaca mulatta*). Am. J. Primatol. 65, 1–25.
Stelkens, R., Seehausen, O., 2009. Genetic distance between species predicts novel trait expression in their hybrids. Evolution 63, 884–897.
Stelkens, R.B., Schmid, C., Selz, O., Seehausen, O., 2009. Phenotypic novelty in experimental hybrids is predicted by the genetic distance between species of cichlid fish. BMC Evol. Biol. 9, 283.
Tattersall, I., Schwartz, J.H., 1999. Commentary hominids and hybrids: The place of Neanderthals in human evolution. Proc. Natl. Acad. Sci. USA 96, 7117–7119.
Tosi, A.J., Morales, J.C., Melnick, D.J., 2000. Comparison of Y chromosome and mtDNA phylogenies leads to unique inferences of macaque evolutionary history. Mol. Phylogenet. Evol. 17, 133–144.
Trevathan, W., 2015. Primate pelvic anatomy and implications for birth. Philos. Trans. Roy. Soc. B Biol. Sci. 370, 20140065.
Trinkaus, E., Milota, Ş., Rodrigo, R., Mircea, G., Moldovan, O., 2003a. Early modern human cranial remains from the Peştera cu Oase, Romania. J. Hum. Evol. 45, 245–253.
Trinkaus, E., Moldovan, O., Milota, Ş., Bîlgăr, A., Sarcina, L., Athreya, S., Bailey, S.E., Rodrigo, R., Mircea, G., Higham, T., Bronk Ramsey, C., Van der Plicht, J., 2003b. An early modern human from the Peştera cu Oase, Romania. Proc. Natl. Acad. Sci. USA 100, 11231–11236.
Warren, K.A., Ritzman, T.B., Humphreys, R.A., Percival, C.J., Hallgrímsson, B., Ackermann, R.R., 2018. Craniomandibular form and body size variation of first generation mouse hybrids: A model for hominin hybridization. J. Hum. Evol. 116, 57–74.
Weaver, T.D., 2009. The meaning of Neandertal skeletal morphology. Proc. Natl. Acad. Sci. USA 106, 16028–16033.
Weaver, T.D., 2014. Quantitative- and molecular-genetic differentiation in humans and chimpanzees: Implications for the evolutionary processes underlying cranial diversification. Am. J. Phys. Anthropol. 154, 615–620.
Weaver, T.D., Hublin, J., 2009. Neandertal birth canal shape and the evolution of human childbirth. Proc. Natl. Acad. Sci. USA 106, 8151.
Weaver, T.D., Stringer, C.B., 2015. Unconstrained cranial evolution in Neandertals and modern humans compared to common chimpanzees. Proc. Royal Soc. B Biol. Sci. 282, 20151519.
Wells, J.C.K., Stock, J.T., 2007. The biology of the colonizing ape. Am. J. Phys. Anthropol. 134, 191–222.
Wolf, A.B., Akey, J.M., 2018. Outstanding questions in the study of archaic hominin admixture. PLoS Genet. 14, e1007349.
Wolfe, L.D., 1986. Reproductive biology of rhesus and Japanese macaques. Primates 27, 95–101.
Zhang, Y.-P., Shi, L.-M., 1993. Phylogeny of rhesus monkeys (*Macaca mulatta*) as revealed by mitochondrial DNA restriction enzyme analysis. Int. J. Primatol. 14, 587–605.
Zirkle, D., Lovejoy, C.O., 2019. The hominid ilium is shaped by a synapomorphic growth mechanism that is unique within primates. Proc. Natl. Acad. Sci. USA 116, 13915–13920.